Synthesis of red mud derived M-type barium hexaferrites with tuneable coercivity

João Carvalheiras[a,*], Rui M. Novais[a], Farzin Mohseni[a,b], João S. Amaral[b], Maria P. Seabra[a], João A. Labrincha[a], Robert C. Pullar[a,**]

[a] *Department of Materials and Ceramic Engineering, CICECO - Aveiro Institute of Materials, University of Aveiro, Campus Universitário de Santiago, 3810-193, Aveiro, Portugal*
[b] *Department of Physics, CICECO, Aveiro Institute of Materials, University of Aveiro, Campus Universitário de Santiago, 3810-193, Aveiro, Portugal*

ARTICLE INFO

ABSTRACT

Hexagonal ferrites can be employed in a multitude of applications, the most common hexaferrites are the M ferrites such as $BaFe_{12}O_{19}$ (barium hexaferrite, BaM). It is known that if Fe^{3+} is substituted with a combination of Ti^{4+}/Co^{2+} the coercivity of BaM can be reduced to produce soft M ferrites with easily switchable magnetisation. They can be utilised as powders, films or bulk ceramics, and can be manufactured from a wide variety of synthesis methods. The production of hexaferrites usually requires commercial raw materials, but if an industrial waste can be utilised, this will help to ease waste disposal and storage costs, valorise a waste material and encourage circular economy. In this study, bauxite residue (red mud) from the production of alumina was used to synthesise M-type hexaferrites, using a simple ceramic process. $BaCO_3$, or $BaCO_3 + Co_3O_4$, were added to the red mud, blended and heated at 1000 °C to produce the M-type hexaferrites. Without cobalt addition up to 81.1 wt% M ferrite was produced, and with Co addition up to 74.3 wt% M ferrite was formed. Without cobalt, the M ferrite phase closely resembled $BaFe_9Al_3O_{19}$, and was a hard ferrite with a magnetisation of 12–19 A m²/kg for the whole powder (up to 23.6 A m²/kg for the M ferrite phase) and a coercivity of ~290 kA/m. When cobalt was added, secondary titanate phases vanished, and Ti^{4+}/Co^{2+} partially substituted very soft M ferrite was formed with a low coercivity of ~16 kA/m but a higher magnetisation of 24.5 A m²/kg for the whole powder (up to 34.9 A m²/kg for the M ferrite phase). Therefore, not only can good quality magnetic materials be easily produced from this common waste material, but its magnetic properties can be tuned by varying the 2 + ions added during the process.

1. Introduction

Iron-rich bauxite waste, red mud, is a well-known waste from alumina production by the Bayer process, consisting mainly of Fe, Al, Ti, Na and Si oxides. It is estimated that up to 1.5 tonnes of red mud are generated to produce 1 tonne of alumina [1–3], in an extremely polluting process, resulting in a global red mud stockpile of around 4 Gt and it is expected that the amount of this waste will increase by a further 146 million tonnes every year [4]. Red mud is considered a hazardous material, because of the toxic metals present, and the Bayer process uses large quantities of sodium hydroxide, making bauxite wastes extremely alkaline. Before the 1970's this type of waste was dumped directly into the sea or stored in land reservoirs [3,5], which is clearly unsustainable and raises severe environmental problems.

Consequently, there is currently a great deal of interest in, and a need for, the reuse and valorisation of this waste stream. As a result of the failure of red mud dams/reservoirs, tragic accidents have occurred in the recent past in Hungry and China, drawing even more attention to the necessity to recycle such wastes [6].

In recent years a paradigm change in the way wastes are viewed, from unwanted by-products to precious raw materials, has led to extensive research attempting to reuse red mud, including applications as red mud as colouring agent in glazes [7,8], as fine aggregate and as aluminosilicate source in concretes and alkali activated materials for structural applications [9–11], as secondary source of Al_2O_3 in porous alkali activated materials for pH regulators [12,13], and as a potential source of metals for metallurgical industries [14,15].

Hexaferrites are a group of iron-based magnetic oxides, and one of

---

the most common magnetic materials used nowadays, with around 300,000 tonnes per year manufactured globally [16], usually from processed oxides, carbonates and minerals. They are used in a widespread variety applications, such as permanent magnets, memories and data storage, electric motors, electronics, microwave and wireless communications devices, stealth technology and radar absorbing materials (RAM), and electromagnetic interference (EMI) shielding at GHz frequencies in electronics and telecommunications [17]. The hexagonal ferrites were first discovered in the 1950's by workers at the Philips Laboratories [18], and they found that M-type ferrites such as $BaFe_{12}O_{19}$ (BaM) have the hexagonal magnetoplumbite structure, and are very hard ferrites, with typical saturation magnetisation (M_s) of 72 A m^2/kg and a coercivity (H_c) of up to 600 kA/m for BaM ceramics [19], although it can be as little as half of this maximum value in non-optimised ceramics. The charge compensated pair of Ti^{+4}/Co^{+2} ions can replace Fe^{3+} in cobalt–titanium substituted M ferrites (Ba-$Co_xTi_xFe_{12-2x}O_{19}$) [17], in which coercivity reduces considerably with substitution, to give very soft ferrites with increasing x [20], while maintaining high magnetisation. The substitution reduces the axial anisotropy until it becomes in-plane at x = 1.3, with reported coercivity values in ceramics as low as 16.0–5.6 kA/m for x = 0.5–1.0 [21,22]. Often, a non-stoichiometric ratio of Fe:Ba between 10 and 11.5 (excess barium) is required to form the single phase BaM ferrite from oxides [17], although this is not always the case [23].

A few previous studies have been performed on the use of wastes as a precursor for hexaferrites. Steel pickling is a surface treatment used to remove impurities and rust from ferrous metals, producing toxic and hazardous wastes containing acids and heavy metals. In the 1990's the ferrites goethite, hematite and magnetite were made from iron oxides recovered from waste steel pickling liquors by Dufour et al., as a cheap source of raw material in a sulphuric acid liquor, and with the high Fe^{2+} content required to produce the spinel ferrites [24]. The same authors also produced BaM with good magnetic properties from these recycled steel pickling liquors [25,26], which were oxidised during oxicoprecipitation at pH 11–12 with a barium salt. They also oxidised and mixed iron rolling scale (steel production) waste with $BaCO_3$ to form a BaM precursor [27], and electroplating wastes (electrolytic slime) have also been processed to produce BaM [28]. However, these were all complicated processes - the highly acidic iron waste had to be oxidised first, and subsequently granulated, mixed with $BaCO_3$ and fired to form the M phase at high temperatures. In the 1980's, electroplating waste slurries contain large amounts of iron hydroxides were mixed with $BaCO_3$ and heated to 1200 °C to form BaM, but as a mixed phase with non-magnetic orthoferrites and spinels [29].

Between 2012 and 2016 Pullar et al. reported on the valorisation of a steel wire drawing waste to make a range of M-type ferrites, such $SrFe_{12}O_{19}$ (SrM) with an addition of $SrCO_3$ [30–32], the cobalt-manganese doped SrM ferrites $SrCo_{0.5}Mn_{0.5}Fe_{11}O_{19}$ and $SrCoMnFe_{10}O_{19}$ with additions of $SrCO_3$, Co_3O_4 and $MnCl_2 \cdot 4H_2O$ [31,32], and BaM with an addition of $BaCO_3$ [33]. All these M ferrites were made from dried sludges by simple solid-state reactions, with no further processing or treatment apart from addition of the 2 + ions, and they formed at relatively low temperatures of around 1000 °C. It was found that with stoichiometric additions of $SrCO_3$ and $BaCO_3$ single phase M ferrites were not formed, but with a nonstoichiometric addition of $BaCO_3$ at a ratio of Fe:Ba of 11:1 the optimum amount (86%) of M ferrite was formed [33]. These M ferrites were investigated as black pigments for colouring glazes and clay bodies, and as magnetic materials, and despite their mixed phases and content of many ions other than Fe^{3+} and Ba^{2+} from the wastes used, they possessed good magnetic properties, suitable for use as permanent magnets despite these impurities. The cobalt-manganese SrM ferrites were very soft magnets, with M_s = 50–60 A m^2/kg and H_c = 12–20 kA/m [32], while the BaM was a hard magnet with M_s = 48 A m^2/kg and H_c up to 300 kA/m [33].

The only other reports of wastes-based hexagonal ferrites are in the last years (2018–2019), of BaM made from unspecified iron oxides

wastes from the steel industry mixed with $BaCO_3$ heated at 1100 °C [34], soft magnetic glass ceramics containing a portion of BaM from a mixture of 50% iron oxide sintering wastes in a glass with a large amount of added $BaCO_3$ [35], and BaM made from dewatered acid mine drainage sludges with added $BaCO_3$ [36], forming at 1100 °C with secondary alumina silicate and calcium sulphate phases (no magnetic data given).

Here, for the first-time red mud was used as a source of Fe to form hexaferrites. The red mud also contains other ions, such as Al^{3+}, Ti^{4+} and Si^{4+} that can substitute Fe^{3+}, and Ca^{2+} which can substitute Ba^{2+}, in the hexaferrite structure. The addition of cobalt to the structure was also studied, as Co^{2+} can compensate for the excess charge when Ti^{4+} substitutes Fe^{3+}. Clearly, the production of such widely used magnetic materials from the valorisation of wastes could be a major advantage, from both economic and sustainability aspects, as well as removing a potential contaminant from the environment.

2. Experimental conditions

2.1. Materials

Iron-rich red mud (RM, 52 wt% of Fe_2O_3) was supplied by an aluminium production industry as a slurry. RM was dried overnight (100 °C), crushed and sieved, and then only particles below 75 μm were used as iron source. Barium carbonate ($BaCO_3$, Sigma-Aldrich ≥ 99.0% pure) and cobalt (II, III) oxide (Co_3O_4, Sigma-Aldrich ≥ 99.8% pure) were used as barium and cobalt sources, respectively.

2.2. Red mud based hexaferrites preparation

Red mud based hexaferrites were produced by mixing RM (10 g) with various amounts of $BaCO_3$ and Co_3O_4 (see Table 1), in a planetary ball mill (Retsch PM400) with alumina balls (~15 mm diameter) in 40 ml of 2-propanol (IPA) for 24 h at 200 rpm. Subsequently, the powders were dried at 120 °C, afterwards, calcined at 1000 °C for 2 h (5 °C/min heating and cooling rates), based on preceding work by the authors [23,33].

2.3. Materials characterisation

The chemical composition of the dried RM was analysed by X-ray fluorescence (XRF, Philips X'Pert Pro MPD), the loss on ignition (LOI) was also assessed at 1000 °C. The presence of crystalline phases was assessed by X-ray diffraction (XRD, Rigaku Geigerflex D/max-Series, Cu Kα radiation, 2θ = 10–80°, scan of 0.02° per step, scan rate of 10 s/step).

The calcined powders were analysed by XRD analysis and scanning electron microscopy (SEM, Hitachi S4100 equipped with energy dispersion spectroscopy, EDS). To evaluate the magnetic properties a superconducting quantum interference device (SQUID, Quantum Design MPMS3) magnetometer was used at 300 K with applied magnetic fields up to 4 T.

Table 1
Mixture proportions of the prepared samples.

Sample ID	Mixture proportion (g)		
	RM	$BaCO_3$	Co_3O_4
RM_1000C	10	0	0
RM + Ba		1.916	0
RM + Ba(Ca)		1.247	0
RM + Ba + Co		2.246	1.706
RM + Ba(Ca) + Co		1.599	1.706

1- Na₅AlCSi₃O₁₅ (00-015-0469)
2- Boehmite (00-021-1307)
3- Gibbsite (04-013-6979)
4- Chantalite (00-029-1410)
5- Hematite (00-033-0664)
6- Anatase (00-021-1272)
7- Quartz (00-046-1045)
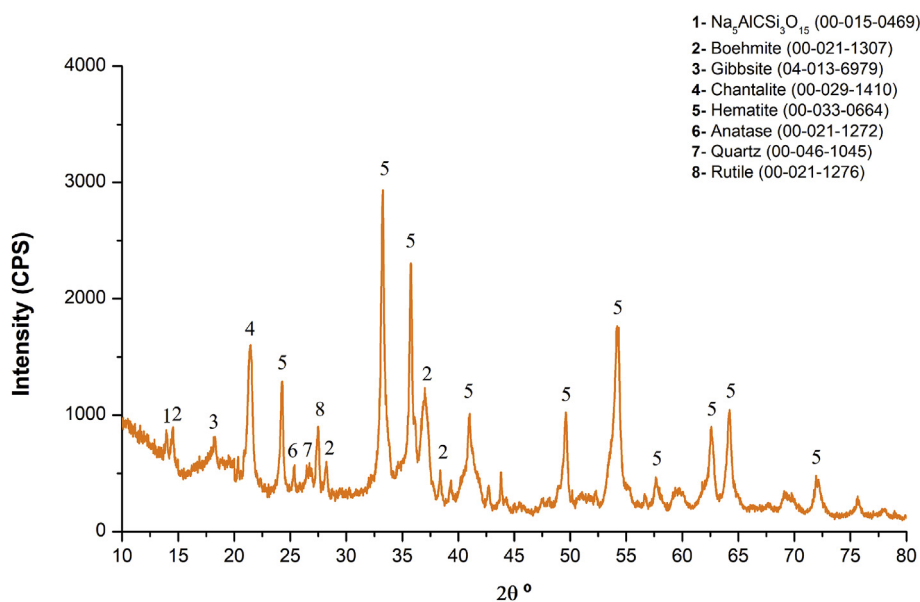**8-** Rutile (00-021-1276)

Fig. 1. XRD pattern from red mud before calcination. (For interpretation of the references to colour in this figure legend, the reader is referred to the Web version of this article.)

3. Results and discussion

3.1. Characterisation of the dried RM and development formulations

XRD results of RM powder is shown in Fig. 1. The major crystalline phase present is hematite (α-Fe_2O_3), which is in accordance with the XRF results. Other minor crystalline phases present are aluminosilicates and titanates, such as boehmite (γ-AlO(OH), gibbsite (Al(OH)₃), chantalite (CaO·Al₂O₃·SiO₂·2H₂O), anatase (β-TiO_2) and rutile (α-TiO_2), quartz (SiO₂) and sodium aluminium silicate carbonate (Na₅Al₃CSi₃O₁₅) which have been found in RM previously [37–39].

Table 2 presents the chemical composition of the dried RM powder determined by XRF (expressed as oxides). The amount of iron oxide is slightly above 52 wt%. Other oxides, namely Al_2O_3, TiO_2 and SiO_2 appear in significant quantities, being about 14.6 wt%, 9.4 wt% and 5.7 wt%, respectively. However, the oxides content should be considered with care, as it might not always correspond to the RM phases. As shown above, the XRD pattern of RM shows the presence of several Al-containing phases, such as boehmite and gibbsite, and not only Al_2O_3.

RM composition is affected by the extraction location, Fe_2O_3 is usually the main component, however, it can vary from 26 to 60 wt% [13,40–43]. The amount of each of the metal ion present in the RM can be calculated from the oxides content determined by XRF. The obtained values are (mol/g): 65.43×10^{-4} Fe^{3+}, 28.71×10^{-4} Al^{3+}, 11.78×10^{-4} Ti^{4+}, 9.43×10^{-4} Si^{4+}, 15.56×10^{-4} Na^{+} and 3.36×10^{-4} Ca^{2+}. In BaM, all of these ions, except sodium ions, can substitute Fe^{3+}. Al^{3+} and Ti^{4+} are well known as potential substitutes for Fe^{3+} in the hexaferrite structure [17]. Si^{4+} is commonly added as a sintering additive as SiO_2 to hexaferrites in sizeable % amounts, where it segregates at the grain boundaries [17], but nevertheless, small levels of Si^{4+} can also substitute for Fe^{3+}, as shown by several studies. It has been reported that SiO_2 is not an inert additive, but a reactive one. Depending on the value of x, it can dissolve in SrM [44], and small amounts of Si^{4+} have substituted Fe^{3+} in M-type hexaferrites [45]. Furthermore, calcium can substitute barium [17], and around 1 mole % Si^{4+} has substituted for Fe^{3+} when charge compensated by Ca^{2+} co-substitution [46,47] or with Co^{2+} [48]. Accounting for the sum of Fe + Al + Ti + Si species present in the RM (134.27×10^{-4} mol/g), it should only be necessary to add 9.61×10^{-4} mol/g of Ba^{2+} to form a pure BaM ferrite if all of these were to substitute for Fe^{3+}. Furthermore, Ca^{2+} can substitute the barium ions, which would render the amount of barium required even smaller (6.26×10^{-4} mol/g). Therefore, two compositions of BaM ferrite were prepared (assuming or not the possibility of calcium for barium substitution): **RM + Ba** with 9.61×10^{-4} mol of $BaCO_3$ (0.1897 g/g of RM); and **RM + Ba(Ca)** with 6.26×10^{-4} mol of $BaCO_3$ (0.1234 g/g of RM). We chose to assume complete substitution, as we wanted to add the minimum amount of added barium, to keep costs down.

However, to compensate unbalanced charge when Ti^{4+} and Si^{4+} replace Fe^{3+}, co-addition of 2 + species of similar size, such as Co^{2+}, is often required [49–51]. The presence of cobalt addition might induce the formation of magnetically soft hexaferrites, such as Co₂Y, a well-known hexaferrite (Ba₂Co₂Fe₁₂O₂₂) known to have lower magnetisation (Ms) when compared with the M Ferrites.

Each gram of RM introduces 21.21×10^{-4} mol of tetravalent species, so 21.21×10^{-4} mol of Co^{2+}/g was also added (0.1702 g/g of RM). A slightly larger quantity of $BaCO_3$ then had to be added to obtain the stoichiometric BaM, again considering or not the barium for calcium substitution in the structure: samples **RM + Ba + Co** and **RM + Ba(Ca) + Co**.

The amounts of precursors used to formulate the four compositions are shown in Table 1. Sodium in the RM might act as a fluxing agent, being concentrated in the intergranular region rather than become incorporated into the ferrite structure. This role was reported in the

Table 2
Chemical composition of the red mud, estimated by XRF (expressed as oxides).

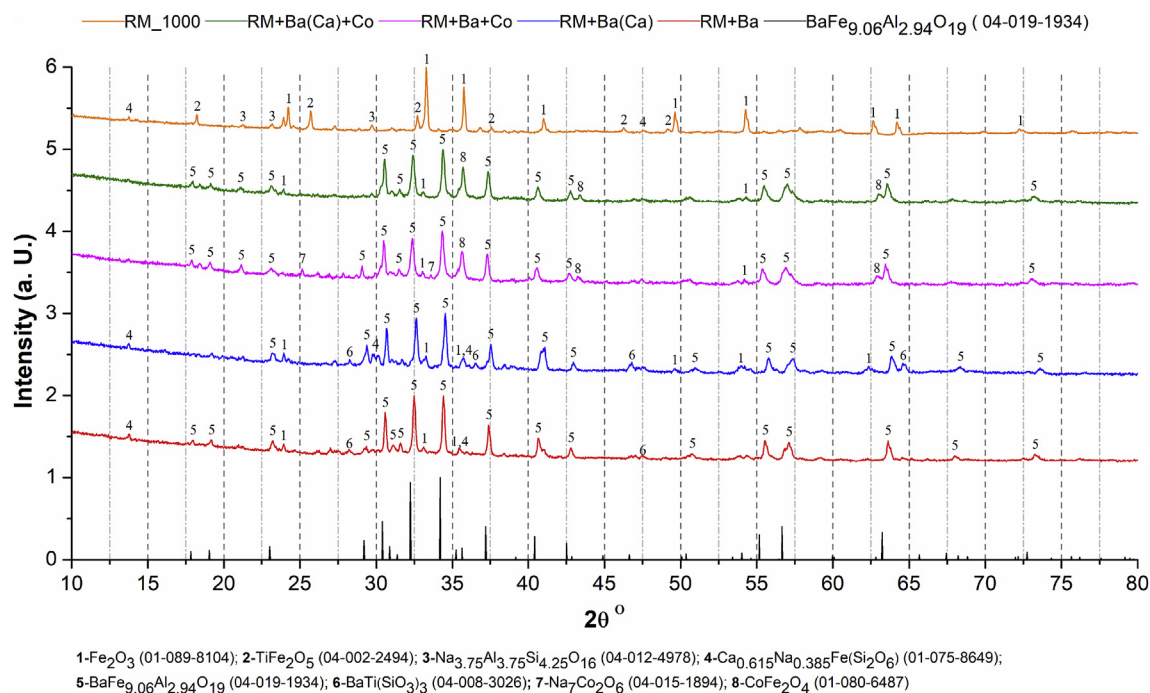| Oxides present	Wt.%
Fe_2O_3	52.25
Al_2O_3	14.63
TiO_2	9.41
SiO_2	5.67
Na_2O	4.82
CaO	1.88
P_2O_5	0.53
SO_3	0.32
K_2O	0.08
MgO	0.08
MnO	0.06
LOI	9.44

Fig. 2. XRD pattern for all powders prepared after calcination at 1000 °C.

preparation of $SrZn_2Fe_{16}O_{27}$ ceramics [52].

3.2. Characterisation of the calcined RM

Fig. 2 shows the XRD pattern of RM calcined at 1000 °C (**RM_1000**). When compared with the dried RM pattern in (Fig. 1), several changes occurred: chantalite (aluminium hydroxide) peak disappeared and was transformed into Al_2O_3 due to dehydration reactions [42]. The same happened with boehmite and gibbsite, as reported by Carneiro et al. [7]. Crystalline phases detected in **RM_1000**, such as $Na_{3.75}Al_{3.75}Si_{4.25}O_{16}$ and $Ca_{0.615}Na_{0.385}Fe(Si_2O_6)$, result from the reaction/combination of Ca, Al, Si and Na. Hematite is also present, although some iron has reacted with titania to form $TiFe_2O_5$ (pseudo-brookite), as is expected when a mixture of TiO_2 and Fe_2O_3 is heated to temperatures around or above 900 °C [53,54]. EDS mapping of the **RM_1000** sample (Fig. 3) shows the distribution of main elements through the microstructure - Fe, Ca, Al, Na and Si.

3.3. RM based hexagonal ferrites

3.3.1. RM-barium carbonate mixtures without cobalt

As can be seen in Fig. 2, the presence of barium in the mixture promotes the formation of a hexagonal M ferrite structure, with characteristic peaks between $2\theta = 30$–38°. The XRD pattern of this M ferrite phase mostly closely resembled the standard JCPDS file for Ba-Fe$_{9.06}$Al$_{2.96}$O$_{19}$ (pattern no. 04-019-1934), which is not surprising as the RM contains a ratio of ~1 Al: 3.6 Fe (calculated form the XRF), and it is known that Al^{3+} can substitute for Fe^{3+} in the M ferrite structure [17]. In fact, lattice parameters were calculated, and as can be seen in Table 3, these results suggest that Al is present in the M ferrite structure, as aluminium substitution leads to a decrease in lattice parameters [55].

In **RM + Ba** the detected secondary phases are: α-Fe$_2$O$_3$, $Ca_{0.615}Na_{0.385}Fe(Si_2O_6)$, rutile and BaTi(SiO$_3$)$_3$. The lower amount of added Ba in **RM + Ba(Ca)** seems to upset the formation of main M ferrite once that some peaks disappear and hematite peaks reappear. This suggests that the calcium has not substituted for barium in the ferrite, along with the coexistence of the calcium containing $Ca_{0.615}Na_{0.385}Fe(Si_2O_6)$ and as a result, less hexaferrite is formed for the compositions with smaller barium content. Otherwise, the two XRD patterns are very similar.

Rietveld refinement supports these results, as it shows that the **RM + Ba** sample contained 81.1 wt % M ferrite, while only 76.5 wt % of M ferrite was in **RM + Ba(Ca)**. A greater amount of $Ca_{0.615}Na_{0.385}Fe(Si_2O_6)$ present in **RM + Ba(Ca)** also supported these results (Table 4).

Fig. 4a) and b) show SEM images of the typical hexagonally shaped platy grains found in M ferrites, with diameters of around 285 nm for **RM + Ba** and 350 nm for **RM + Ba(Ca)**.

3.3.2. RM-barium carbonate mixtures with cobalt

The samples containing cobalt still appear to form an M ferrite as the major crystalline phase (Fig. 2) with lattice parameters close to the samples without cobalt (see Table 3). This also suggests that no other type of hexaferrite was formed, as they tend to have larger unit cells and, hence, a greater lattice parameter c [17], although, as it will be seen in the magnetic data in section 3.4, the addition of cobalt promoted a major change in this phase. The appearance of a large spinel ferrite peak is also observed, which resembles that for $CoFe_2O_4$, although all the spinel patterns are very similar. The other significant difference is the absence of most of the secondary phases: $Ca_{0.615}Na_{0.385}Fe(Si_2O_6)$, TiO_2 and BaTi(SiO$_3$)$_3$. This suggest that the addition of cobalt has led to the formation of a spinel ferrite phase, which may accommodate all elements present in such phases. The co-incorporation of Ti^{4+} and Co^{2+} species into the M ferrite structure (for charge compensation), may lead to freeing the iron to form the spinel phase. Despite this, a trace of α-Fe$_2$O$_3$ are still visible (Fig. 2).

This is again supported by Rietveld refinement. In Table 4 can be seen that the main phase present for both samples is the M ferrite phase, above 70 wt % for both samples, as well as formation of the secondary phases reported above.

In general, there are no major differences between **RM + Ba + Co** and **RM + Ba(Ca) + Co** samples, excepting the presence of $Na_7Co_2O_6$ in **RM + Ba + Co**. There are reports of iron slags which contain cobalt, calcium and silicon ions, and which can form the spinel structure [56].
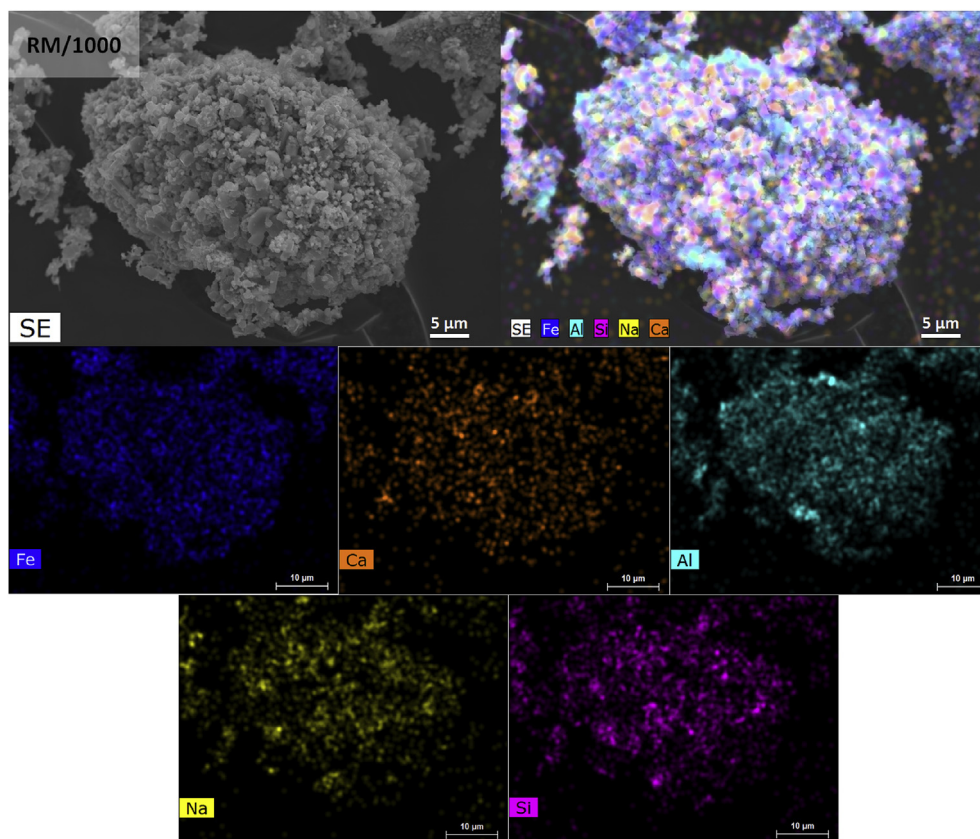
Fig. 3. EDS map for Red mud calcined at 1000 °C. (For interpretation of the references to colour in this figure legend, the reader is referred to the Web version of this article.)

Table 3
Experimental lattice parameters calculated.

	a (Å)	c (Å)
RM + Ba	5.846	23.004
RM + Ba(Ca)	5.824	22.887
RM + Ba + Co	5.855	23.057
RM + Ba(Ca) + Co	5.846	23.040

As can be seen in Fig. 4c) and d), the grains of these ferrites also have a less hexagonal appearance and are smaller, with diameters of around 180 nm for RM + Ba + Co and 170 nm for RM + Ba(Ca) + Co.

3.4. Magnetic properties

The magnetic hysteresis loops of **RM_1000** and RM derived hexaferrites are shown in Fig. 5, and their values given in Table 5. As would be expected from a material with no significant magnetic phases, the RM is virtually non-magnetic even after calcination at 1000 °C, with a very small magnetisation (M_s) of 1 A m^2/kg under an applied field of 4 T, but a relatively large coercivity (H_c) of ~200 kA/m. This hard

magnetisation means it is conceivable that a very small amount of M ferrite, or a hard spinel phase, has formed, but its amount is too small to be detected by XRD, and will have no significant effect on the properties of the major magnetic phase.

In **RM + Ba**, in which a stoichiometric amount of Ba was added to the total quantity of (Fe + Al + Ti + Si) ions, the loop clearly has the form which would be expected from a hard M ferrite sample, with the straight, parallel sides of the loop indicating that there is no significant secondary magnetic phase present. H_c is high at ~287 kA/m, but the M_s value is low for an M ferrite, at 19.1 A m^2/kg. However, this value is for the whole powder sample – if only the 81.1 wt% M ferrite magnetic phase is considered, it has an estimated M_s of 23.6 A m^2/kg. This is typical for BaM when Fe^{3+} is substituted by nonmagnetic ions such as Al^{3+}, Ti^{4+} and Si^{4+}, as is the case here, with the total number of these nonmagnetic ions (49.92×10^{-4} mol/g) equalling about 70% of the number of magnetic Fe ions (65.43×10^{-4} mol/g). For example, M_s is reported as being only 30.2 A m^2/kg for $BaAl_2Fe_{10}O_{19}$ [57], ~22 A m^2/kg for $BaAl_{2.5}Fe_{9.5}O_{19}$ [58], 45 A m^2/kg in $BaCoTiFe_{10}O_{19}$ [59] (in which H_c also decreases), and only 42 and 29 A m^2/kg for $BaAl_{2.5}Fe_{9.5}O_{19}$ and $BaAl_{3.5}Fe_{8.5}O_{19}$, respectively, with H_c ~170 kA/m for both [60]. In a study of Al substituted SrM, it was found that

Table 4
Rietveld refinement for the samples prepared (wt. %).

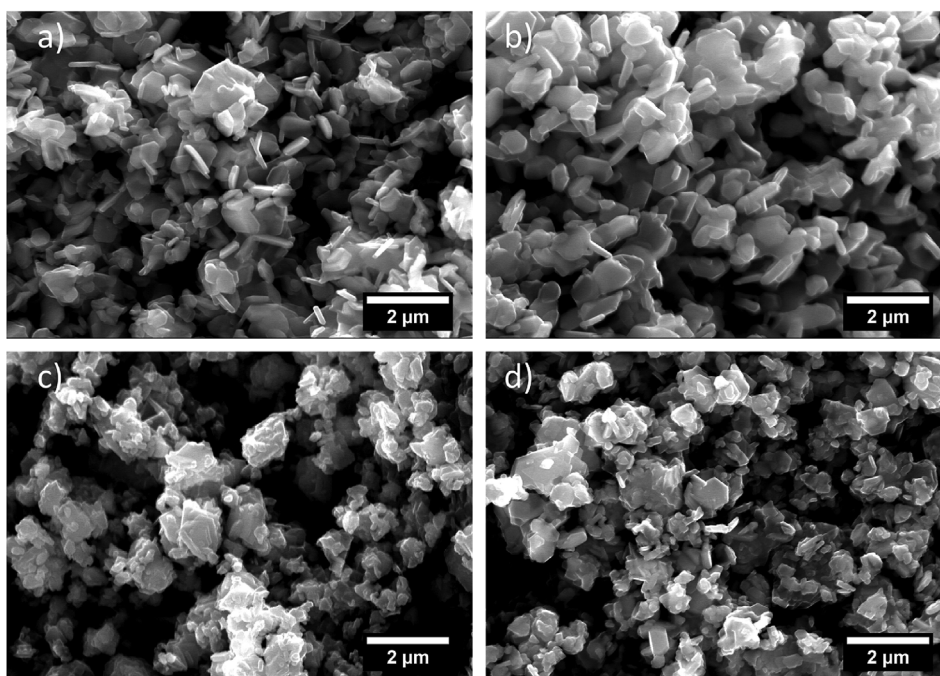|	RM + Ba	RM + Ba(Ca)	RM + Ba + Co	RM + Ba(Ca) + Co
M ferrite	81.09	76.54	70.19	74.34
Fe_2O_3	8.76	6.92	5.19	10.85
$Na_7Co_2O_6$	–	–	19.58	–
$CoFe_2O_4$	–	–	5.03	14.80
$BaTi(SiO_3)_3$	3.14	0.99	–	–
$Ca_{0.615}Fe_{0.385}(Si_2O_6)$	7.01	15.56	–	–

Fig. 4. SEM images taken at 25 kV a) RM + Ba b) RM + Ba(Ca) c) RM + Ba + Co d) RM + Ba(Ca) + Co.
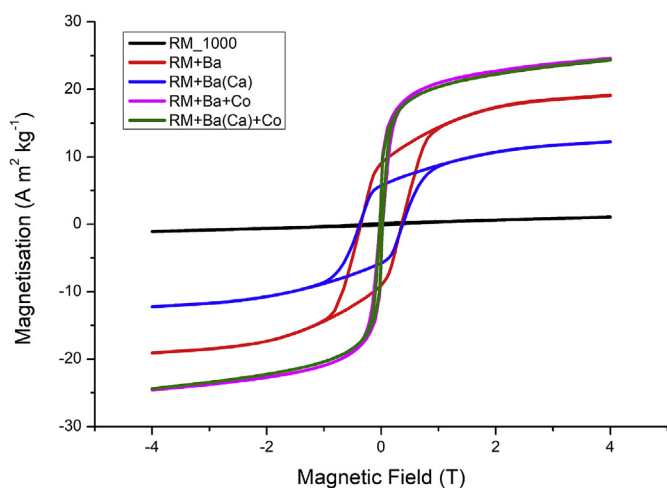

Fig. 5. Magnetic hysteresis loops (at room temperature) for the red mud calcined at 1000 °C, and the RM-derived hexaferrites at 1000 °C. (For interpretation of the references to colour in this figure legend, the reader is referred to the Web version of this article.)

Table 5
Remnant magnetisation (Mr), saturation magnetisation (Ms) and coercivity (Hc) for all the samples prepared. The M_s of BaM is a weight-corrected value considering only the magnetic BaM phase, to give a more accurate value for this ferrite itself.

	M_r (A m^2/ kg)	M_s (A m^2/ kg)	M_s of BaM (A m^2/kg)	H_c (kA/ m)
RM_1000C	0.12	1.0	–	200
RM + Ba	9.1	19.1	23.6	287
RM + Ba(Ca)	5.7	12.1	15.8	295
RM + Ba + Co	4.3	24.5	34.9	16
RM + Ba(Ca) + Co	4.1	24.5	33.0	16

$SrAl_3Fe_9O_{19}$, H_c reached a maximum of 1343 kA/m as M_s had decreased to ~18 A m^2/kg, while $SrAl_4Fe_8O_{19}$ was very poorly magnetic, with H_c ~500 kA/m but a very low M_s of only ~4 A m^2/kg [61]. Another study of Al substituted SrM gave values of M_s = 36.5 and 9.0 A m^2/kg for $SrAl_2Fe_{10}O_{19}$ and $SrAl_4Fe_8O_{19}$, respectively [62]. There are, however, studies where Al and Ca were introduced into a SrM ferrite structure to achieve a H_c of ~1695 kA/m for $Sr_{0.67}Ca_{0.33}Fe_8Al_4O_{19}$ [55] and a massive maximum of ~2870 kA/m for $Sr_{0.54}Ca_{0.46}Fe_{6.5}Al_{5.5}O_{19}$ [63].

Therefore, although we cannot definitely say what the composition is of this BaM ferrite, we can estimate that it has a considerable content of nonmagnetic 3 + and 4 + ions, and this would consequently greatly reduce its magnetisation. Nevertheless, the magnetisation is still enough for use as a commercial hard magnet powder and sintered magnet for economic and everyday functions, especially considering its simple production from a waste material which has currently a terrific environmental impact.

RM + Ba(Ca) has an even lower magnetisation of only 12.1 A m^2/ kg for the whole powder (estimated as 15.8 A m^2/kg for the 76.5 wt% M ferrite phase), and indeed its XRD profile indicated more non-magnetic hematite. Its coercivity was slightly larger at 295 kA/m^{-1}, perhaps due to its slightly larger hexagonal grain diameter. As M ferrites approach the single magnetic domain size of ~0.5–1 μm, their coercivity typically increases [17]. This further indicates that calcium is not incorporated into the hexaferrite structure, and that a stoichiometric amount of Ba^{2+} should be added to the combined (Fe^{3+} + Al^{3+} + Ti^{4+} + Si^{4+}).

When cobalt ions are added to the RM as well, it produces a very different result. In both **RM + Ba + Co** and **RM + Ba(Ca) + Co**, a very soft ferrite was produced, with a low coercivity of only ~16 kA/m in both cases (Fig. 5 and Table 5). However, both powders also had higher magnetisation values of 24.5 A m^2/kg. The estimated M_s values of the M ferrite phase alone were 34.9 A m^2/kg in **RM + Ba + Co**, and 33.0 A m^2/kg in **RM + Ba(Ca) + Co**, although it should be noted that these powders also probably contained a second magnetic phase (see below), so these values may be unreliable. These samples did not contain the non-magnetic $Ca_{0.615}Na_{0.385}Fe(Si_2O_6)$, TiO_2 or $BaTi(SiO_3)_3$ phases. However, they contained an unidentified spinel phase, which is also probably magnetic. The XRD pattern of this spinel phase resembled that of $CoFe_2O_4$, which is a hard magnet with a high coercivity. The spinel phases are extremely difficult to tell apart from XRD patterns

alone, and most spinels are soft magnets, such as magnetite, Fe_3O_4. It is likely that this spinel is in fact a mixed spinel also containing Ca^{2+} and Si^{4+} ions from the secondary phases which existed prior to cobalt addition, and as such it would be expected to have greatly reduced coercivity and magnetisation values compared to $CoFe_2O_4$. The slight widening of the magnetic hysteresis loops seen in these samples at low applied fields is typical of a material which contains more than one magnetic phase. The M ferrite phase has also become magnetically soft due to the substitution of the charge compensated Co^{2+}/Ti^{4+} ion pair for Fe^{3+} in the hexaferrite structure, which typically results in a soft M ferrite with coercivity as low as 5–16 kA/m for substitution levels of x = 0.5–1.0 in $BaCo_xTi_xFe_{12-2x}O_{19}$ [21,22].

This signifies that the magnetic properties of the hexaferrite produced from the valorisation of RM wastes can be tuned to be either hard or soft, depending on the desired applications, by selecting the addition of additional 2 + metal cations.

4. Conclusions

When heated to 1000 °C, the red mud produced a virtually nonmagnetic material consisting mostly of α-Fe_2O_3, $FeTi_2O_5$, $Na_{3.75}Al_{3.75}Si_{4.25}O_{16}$ and $Ca_{0.615}Na_{0.385}Fe(Si_2O_6)$, as the phases detected by XRD. However, when a stoichiometric amount of Ba^{2+} was added relative to the total trivalent/tetravalent metal ions ($Fe^{3+} + Al^{3+} + Ti^{4+} + Si^{4+}$), an M-type hexaferrite resulted as the major phase (which probably contains Al^{3+} ions, with the estimated formula being close to $BaFe_9Al_3O_{19}$), with an estimated magnetisation of 23.6 A m^2/kg and a high coercivity (~290 kA/m). The M_s of the whole powder was 19.1 A m^2/kg. If Co^{2+} is also added for charge balancing of Ti^{4+} (and possibly Si^{4+}) present in the RM, the Ti-, Ca- and Si-containing secondary phases disappeared, and a magnetically soft M hexaferrite with a low coercivity (16 kA/m) but a higher magnetisation (estimated up to 34.9 A m^2/kg) was produced, co-existing with a magnetically soft spinel phase. The M_s of the whole powder was 24.5 A m^2/kg. Such a low coercivity is typical of Co^{2+}/Ti^{4+} substituted BaM ferrites. This demonstrates that not only can a potentially valuable magnetic material be easily produced from RM, but that its magnetic properties can also be tuned by the selection of the 2 + cations added. Simply by adding cobalt to the composition, a very soft ferrite is obtained, while in its absence a magnetically hard M hexaferrite with relatively large coercivity is observed.

Declaration of competing interest

The authors declare that they have no known competing financial interests or personal relationships that could have appeared to influence the work reported in this paper.

Appendix A. Supplementary data

Supplementary data to this article can be found online at https://doi.org/10.1016/j.ceramint.2019.11.025.

References

[1] M.A. Khairul, J. Zanganeh, B. Moghtaderi, The composition, recycling and utilisation of Bayer red mud, Resour. Conserv. Recycl. 141 (2019) 483–498 Feb.

[2] N. Ye, Y. Chen, J. Yang, S. Liang, Y. Hu, J. Hu, S. Zhu, W. Fan, B. Xiao, Transformations of Na, Al, Si and Fe species in red mud during synthesis of one-part geopolymers, Cement Concr. Res. 101 (2017) 123–130 Nov.

[3] G. Power, M. Gräfe, C. Klauber, Bauxite residue issues: I. Current management, disposal and storage practices, Hydrometallurgy 108 (1–2) (2011) 33–45 Jun.

[4] K. Evans, The history, challenges, and new developments in the management and use of bauxite residue, J. Sustain. Metall. 2 (4) (2016) 316–331 Dec.

[5] V. Dethlefsen, H. Rosenthal, Problems with dumping of red mud in shallow waters. A critical review of selected literature, Aquaculture 2 (1973) 267–280 Jan.

[6] K. Hammond, 'Recovery of Value-Added Products from Red Mud and Foundry Bag-House Dust', Thesis, Colorado School of Mines, Arthur Lakes Library, 2007.

[7] J. Carneiro, D.M. Tobaldi, W. Hajjaji, M.N. Capela, R.M. Novais, M.P. Seabra, J.A. Labrincha, Red mud as a substitute coloring agent for the hematite pigment, Ceram. Int. 44 (4) (2018) 4211–4219 Mar.

[8] J. Carneiro, M.N. Capela, D.M. Tobaldi, R.M. Novais, M.P. Seabra, J.A. Labrincha, Red mud and electroplating sludge as coloring agents of distinct glazes: the influence of heat treatment, Mater. Lett. 223 (2018) 166–169 Jul.

[9] P. Krivenko, O. Kovalchuk, A. Pasko, T. Croymans, M. Hult, G. Lutter, N. Vandevenne, S. Schreurs, W. Schroeyers, Development of alkali activated cements and concrete mixture design with high volumes of red mud, Constr. Build. Mater. 151 (2017) 819–826 Oct.

[10] W.C. Tang, Z. Wang, Y. Liu, H.Z. Cui, Influence of red mud on fresh and hardened properties of self-compacting concrete, Constr. Build. Mater. 178 (2018) 288–300 Jul.

[11] P.J. Joyce, T. Hertel, A. Goronovski, A.H. Tkaczyk, Y. Pontikes, A. Björklund, Identifying hotspots of environmental impact in the development of novel inorganic polymer paving blocks from bauxite residue, Resour. Conserv. Recycl. 138 (2018) 87–98 Nov.

[12] R.M. Novais, J. Carvalheiras, M.P. Seabra, R.C. Pullar, J.A. Labrincha, Innovative application for red mud-based inorganic polymer spheres as pH regulators, J. Hazard Mater. 358 (2018) 69–81 Sep.

[13] G. Ascensão, M.P. Seabra, J.B. Aguiar, J.A. Labrincha, Red mud-based geopolymers with tailored alkali diffusion properties and pH buffering ability, J. Clean. Prod. 148 (2017) 23–30. Apr.

[14] Z. Liu, H. Li, 'Metallurgical process for valuable elements recovery from red mud—a review', Hydrometallurgy 155 (2015) 29–43 May.

[15] G. Alkan, B. Yagmurlu, S. Cakmakoglu, T. Hertel, S. Kaya, L. Gronen, S. Stopic, B. Friedrich, Novel approach for enhanced scandium and titanium leaching efficiency from bauxite residue with suppressed silica gel formation, Sci. Rep. 8 (1) (2018) Dec.

[16] Ü. Özgür, Y. Alivov, H. Morkoç, Microwave ferrites, part 1: fundamental properties, J. Mater. Sci. Mater. Electron. 20 (9) (2009) 789–834 Sep.

[17] R.C. Pullar, Hexagonal ferrites: a review of the synthesis, properties and applications of hexaferrite ceramics, Prog. Mater. Sci. 57 (7) (2012) 1191–1334 Sep.

[18] J. Smit, H.P.J. Wijn, Ferrites. Eindhoven, Philips technical library, The Netherlands, 1959.

[19] J.J. Went, G.W. Rathenau, E.W. Gorter, G.W. Van Oosterhout, Ferroxdure. a class of new permanent magnet materials, Philips Tech. Rev. 13 (1952) 361.

[20] O. Kubo, T. Ido, H. Yokoyama, Properties of Ba ferrite particles for perpendicular magnetic recording media, IEEE Trans. Magn. 18 (6) (1982) 1122–1124.

[21] M. Fujita, K. Kakizaki, N.H. Ratsuka, K. Haneda, In: Ferrites, Proc ICF6, Tokyo and Kyoto, (1992), p. 968.

[22] C. Singh, S.B. Narang, I.S. Hudiara, Y. Bai, K. Marina, Hysteresis analysis of Co–Ti substituted M-type Ba–Sr hexagonal ferrite, Mater. Lett. 63 (2009) 1921–1924.

[23] R.C. Pullar, A.K. Bhattacharya, Crystallisation of hexagonal M ferrites from a stoichiometric sol–gel precursor, without formation of the α-BaFe2O4 intermediate phase, Mater. Lett. 57 (3) (2002) 537–542.

[24] J. Dufour, L. López, A. Formoso, C. Negro, R. Latorre, F. López-Mateos, Mathematical model of goethite synthesis by oxyprecipitation of steel pickling liquors, Chem. Eng. J. Biochem. Eng. J. 59 (3) (1995) 287–291 Nov.

[25] J. Dufour, R. Latorre, C. Negro, E.M. Alcalá, A. Formoso, F. López-Mateos, Protocol for the synthesis of Ba-hexaferrites with prefixed coercivities, J. Magn. Magn. Mater. 172 (3) (1997) 308–316. Aug.

[26] J. Dufour, R. Latorre, E.M. Alcalá, C. Negro, A. Formoso, F. López-Mateos, Synthesis of M-type hexaferrites from steel pickling liquors (ID 109), J. Magn. Magn. Mater. 157–158 (1996) 125–126 May.

[27] B. Aragón, O. Arés, O. Montesino, J. Dufour, C. Hart, J. Balmaseda, A. Formoso, A. Cores, Obtención de hexaferrita de bario anisotrópica a partir de un residuo siderúrgico, Rev. Metal. 38 (2) (2002) 94–99. Apr.

[28] L.A. Petrukhno, V.M. Makarov, Z.A. Novikova, A.M. Shipilin, I.N. Zakharova, Barium ferrite prepared from electrolytic slime for use in flaw detection, Ind. Lab. 65 (3) (1999) 167–169.

[29] A.S. Vlasov, I.G. Stepanchikova, S.V. Makarov, V.A. Zaitsev, A.S. Danilov, Barium hexaferrite based on the waste products from electroplating processes, Glass Ceram. 44 (4) (1987) 135–137. Apr.

[30] W. Hajjaji, R.C. Pullar, C. Zanelli, M.P. Seabra, M. Dondi, J.A. Labrincha, Compositional and chromatic properties of strontium hexaferrite as pigment for ceramic bodies and alternative synthesis from wiredrawing sludge, Dyes Pigments 96 (3) (2013) 659–664 Mar.

[31] W. Hajjaji, R. Pullar, M.P. Seabra, J.A. Labrincha, Chromatic properties of industrial solid waste based ferrites, Waste Biomass Valorization 3 (3) (2012) 375–378 Sep.

[32] R.C. Pullar, W. Hajjaji, J.S. Amaral, M.P. Seabra, J.A. Labrincha, Magnetic properties of ferrite ceramics made from wastes, Waste Biomass Valorization 5 (1) (2014) 133–138 Feb.

[33] R.C. Pullar, M. Saeli, R.M. Novais, J.S. Amaral, J.A. Labrincha, Valorisation of industrial iron oxide waste to produce magnetic barium hexaferrite, ChemistrySelect 1 (4) (2016) 819–825. Apr.

[34] N. Idayanti, Dedi, T. Kristiantoro, D. Mulyadi, N. Sudrajat, G.F.N. Alam, Manufacture of barium hexaferrite (BaO3.98Fe$_2$O$_3$) from iron oxide waste of grinding process by using calcination process, J. Phys. Conf. Ser. 985 (2018) 012048Mar.

[35] S.A.M. Abdel-Hameed, I.H. M, N.A. Erfan, Recycling of iron sintered wastes into nanoparticles barium hexaferrite and zinc-ferrite glass-ceramics, Silicon 10 (1) (2018) 153–163 Jan.

[36] M. Liu, A. Iizuka, E. Shibata, Acid mine drainage sludge as an alternative raw material for M-type hexaferrite preparation, J. Clean. Prod. 224 (2019) 284–291 Jul.

[37] D.V. Ribeiro, J.A. Labrincha, M.R. Morelli, Potential use of natural red mud as pozzolan for Portland cement, Mater. Res. 14 (1) (2011) 60–66 Jan.

[38] M. Ghita, F. Stoiciu, V. Badilita, Lenuta Enache, M. Stoiciu, Mineralogical and chemical study of the hydrargillitic bauxite and of the red mud resulted as by-product for its revaluation, Proceedings of 11th International Multidisciplinary Scientific GeoConference, Albena, Bulgaria, 19-25th June 2011, Vol. 1 June 2011, pp. 1–7, , https://doi.org/10.13140/2.1.3182.0481.

[39] Y. Pontikes, Red mud project - characteristics, 02-May-2005. [Online]. Available: http://redmud.org/red-mud/characteristics/ , Accessed date: 15 May 2019.

[40] J. Pera, R. Boumaza, J. Ambroise, Development of a pozzolanic pigment from red mud, Cement Concr. Res. 27 (10) (1997) 1513–1522 Oct.

[41] V.M. Sglavo, R. Campostrini, S. Maurina, G. Carturan, M. Monagheddu, G. Budroni, G. Cocco, Bauxite "red mud" in the ceramic industry. Part 1: thermal behaviour, J. Eur. Ceram. Soc. 20 (3) (2000) 235–244 Mar.

[42] H. Sutar, Progress of red mud utilization: an overview, Am. Chem. Sci. J. 4 (3) (2014) 255–279 Jan.

[43] S. Srikanth, A.K. Ray, A. Bandopadhyay, B. Ravikumar, A. Jha, Phase constitution during sintering of red mud and red mud-fly ash mixtures, J. Am. Ceram. Soc. 88 (9) (2005) 2396–2401 Sep.

[44] F. Kools, Action of silica additive during sintering of strontium hexaferrite. Part I: preparation and examination of sintered materials, the chemical action of silica, grain growth inhibition by precipitate drag, Sci. Sinter. 17 (1–2) (1985) 49–62.

[45] C.-C. Huang, A.-H. Jiang, Y.-H. Hung, C.-H. Liou, Y.-C. Wang, C.-P. Lee, T.-Y. Hung, C.-C. Shaw, M.-F. Kuo, C.-H. Cheng, Influence of CaCO$_3$ and SiO$_2$ additives on magnetic properties of M-type Sr ferrites, J. Magn. Magn. Mater. 451 (2018) 288–294.

[46] H. Yamamoto, T. Mitsuoka, Effect of CaO and SiO$_2$ additives on magnetic properties of SrZn$_2$W type hexagonal ferrite, IEEE Trans. Magn. 30 (1994) 5001–5007.

[47] H. Yamamoto, A. Ishii, Effect of CaO and SiO$_2$ addition on magnetic properties of anisotropic Ba-Zn system W-type hexagonal ferrite magnets, Electr. Eng. Japan 114 (1994) 1–8.

[48] E.D. Solovyova, E.V. Pashkova, V.P. Ivanitski, O.I. V'yunov, A.G. Belous, Mössbauer and X-ray diffraction study of Co^{2+}–Si^{4+} substituted M-type barium hexaferrite BaFe$_{12-2x}$Co$_x$Si$_x$O$_{19}$ ± γ, J. Magn. Magn. Mater. 330 (2013) 72–75.

[49] C.C. Huang, A.H. Jiang, Y.H. Hung, C.H. Liou, Y.C. Wang, C.P. Lee, T.Y. Hung, C.C. Shaw, M.F. Kuo, C.H. Cheng, Influence of CaCO3 and SiO2 additives on

magnetic properties of M-type Sr ferrites, J. Magn. Magn. Mater. 451 (2018) 288–294. Apr.

[50] E.D. Solovyova, E.V. Pashkova, V.P. Ivanitski, O.I. V'yunov, A.G. Belous, Mössbauer and X-ray diffraction study of Co2+–Si4+ substituted M-type barium hexaferrite BaFe12−2xCoxSixO19 ± γ, J. Magn. Magn. Mater. 330 (2013) 72–75 Mar.

[51] H. Yamamoto, T. Mitsuoka, Effect of CaO and SiO2 additives on magnetic properties of SrZn2-W type hexagonal ferrite, IEEE Trans. Magn. 30 (6) (1994) 5001–5007 Nov.

[52] H. Nishio, H. Yamamoto, Magnetic viscosity of Sr-Na-Zn W-type hexagonal ferrite magnets, J. Phys. IV 07 (C1) (1997) C1-317–C1-318 Mar.

[53] C. Chen, B.R. Müller, O.I. Lebedev, F. Giovannelli, G. Bruno, F. Delorme, Effects of impurities on the stability of the low thermal conductivity in Fe2TiO5 ceramics, Mater. Char. 149 (2019) 111–117 Mar.

[54] A.M. Al-Saie, A. Al-Shater, S. Arekat, A. Jaffar, M. Bououdina, 'Effect of annealing on the structure and magnetic properties of mechanically milled TiO2–Fe2O3 mixture', Ceram. Int. 39 (4) (2013) 3803–3808 May.

[55] L.A. Trusov, E.A. Gorbachev, V.A. Lebedev, A.E. Sleptsova, I.V. Roslyakov, E.S. Kozlyakova, A.V. Vasiliev, R.E. Dinnebier, M, J, P.E. Kazin, Ca–Al double-substituted strontium hexaferrites with giant coercivity, Chem. Commun. 54 (5) (2018) 479–482.

[56] S. Jahanshahi, S. Sun, F. Kongoli, K. Itagaki, C. Yamauchi, H.Y. Sohn (Eds.), Some Aspects of Calcium Ferrite Slags", Yazawa International Symposium, Metallurgical and Materials Processing Principles and Technologies, Vol. 1: Materials Processing Fundamentals and New Technologies, TMS (The Minerals, Metals & Materials Society), 2003, pp. 227–244.

[57] J. Zhou, H. Ma, M. Zhong, G. Xu, Z. Yue, Z. He, Influence of Co–Zr substitution on coercivity in Ba ferrites, J. Magn. Magn. Mater. 305 (2) (2006) 467–469 Oct.

[58] S. Mahadevan, C. Pahwa, S.B. Narang, P. Sharma, Structural, dielectric and magnetic properties of BaFe 12−x Al x O 19 hexaferrite thick films, J. Magn. Magn. Mater. 441 (2017) 465–474 Nov.

[59] M. Fujita, K. Kakizaki, N.H. Ratsuka, K. Haneda, Ferrites, Proc. ICF6, Tokyo and Kyoto 1992, 1992, p. 968.

[60] S.M. El-Sayed, T.M. Meaz, M.A. Amer, H.A. El Shersaby, Magnetic behavior and dielectric properties of aluminum substituted M-type barium hexaferrite, Phys. B Condens. Matter 426 (2013) 137–143 Oct.

[61] H.Z. Wang, Y.N. Hai, B. Yao, Y. Xu, L. Shan, L. Xu, J.L. Tang, Q.H. Wang, Tailoring structure and magnetic characteristics of strontium hexaferrite via Al doping engineering, J. Magn. Magn. Mater. 422 (2017) 204–208 Jan.

[62] H. Luo, B.K. Rai, S.R. Mishra, V.V. Nguyen, J.P. Liu, Physical and magnetic properties of highly aluminum doped strontium ferrite nanoparticles prepared by auto-combustion route, J. Magn. Magn. Mater. 324 (17) (2012) 2602–2608. Aug.

[63] E.A. Gorbachev, L.A. Trusov, A.E. Sleptsova, E.S. Kozlyakova, L.N. Alyabyeva, S.R. Yegiyan, A.S. Prokhorov, V.A. Lebedev, I.V. Roslyakov, A.V. Vasiliev, P.E. Kazin, Hexaferrite Materials Displaying Ultra-high Coercivity and Sub-terahertz Ferromagnetic Resonance Frequencies', Mater. Today, Corrected Proof, (2019) online 18th June.